Journal of Andrology, Vol. 22, No. 4, July/August 2001

Measurement of Bovine Sperm Nuclear Shape Using Fourier Harmonic Amplitudes

G. CHARLES OSTERMEIER,* GLEN A. SARGEANT,† BRIAN S. YANDELL,‡ AND JOHN J. PARRISH*

*From the Departments of *Animal Sciences, †Wildlife Ecology, and ‡Statistics and Horticulture, University of Wisconsin-Madison, Madison, Wisconsin.*

ABSTRACT: An objective method for measuring bovine sperm nuclear shape was developed. Digital images of bovine sperm stained with propidium iodide were collected and Fourier functions used to describe the perimeters of individual sperm nuclei. Harmonic amplitudes from Fourier functions were first shown to be independent of sperm orientation during digitization. Sperm from 12 different bulls were used, and 6 harmonic amplitudes per sperm were found to adequately describe sperm nuclear shape. Based on harmonic amplitudes 0 to 5, cluster analysis was used to generate 20 different groups. Sperm within groups had similar morphologies and groups were distinguished by statistically unique shape characteristics. Harmonic amplitudes 0 to 5 can be used to distinguish previously reported abnormalities such as tapered, pyriform, macrocephalic, and microcephalic, as well as gradations in between. Furthermore, differences were detected among bull harmonic amplitude centroids ($P < .05$), indicating that bulls differ in mean sperm nuclear shape.

Key words: Sperm morphology, computer-aided image analysis, CASA.

J Androl 2001;22:584–594

Evaluation of some semen quality parameters can be done objectively. For example, volumetric measurement can be used to determine semen volume, spectrophotometry to establish sperm concentration (Salisbury et al, 1943; Willet and Buckner, 1951), and motion analysis (Katz and Davis, 1987) or multiple exposure photography (Makler, 1978) to assess sperm motility. In contrast, evaluation of sperm morphology generally relies on subjective microscopic examination of semen (Barth and Oko 1989; Ferrari et al, 1998; Johnson et al, 1998; Lim et al, 1998; Berkovitz et al, 1999). Multiple observers can classify the same sperm differently, depending on their interpretations of normal and abnormal morphology (Dunphy et al, 1989; Neuwinger et al, 1990). The same observer may even classify the same sperm differently on successive occasions. The purpose of semen evaluation is to identify poor-quality ejaculates, or ejaculates suspected of having low fertility. Once identified, these samples are discarded. Therefore, accuracy and repeatability are a must to ensure that only high-quality ejaculates are retained and that only poor-quality ejaculates are discarded.

Several attempts have been made to objectively assess sperm head morphology through computer-aided image analysis. Such methods have typically relied on measures of area, perimeter, length, width, or combinations of these (Auger and Dadoune, 1993; Gravance et al, 1996; Park et al, 1997; Aziz et al, 1998). Initially, these measures may be attractive for shape analysis but, ultimately, they are inappropriate because they primarily reflect variation in size rather than shape (Young et al, 1974; Diaz et al, 1989). Consequently, these measures do not adequately reflect the variation commonly observed in sperm head shape. Another approach has been to measure bending energy and normalized, mean absolute curvature (Sailer et al, 1996). These measures combine several aspects of shape to explain the amount of energy required at a specific point to form a given contour from a straight line. Sensitivity is lost, however, by combining large amounts of information into one measure of shape.

Humans can distinguish subtle differences in shape (Atteneave, 1954; Atteneave and Arnoult, 1966) by focusing on perimeter regions that possess high curvature. These regions are also used by humans to categorize and reproduce the shape of specific objects. Accordingly, methods for measuring sperm head shape should also depend on these criteria. Fourier harmonic analysis of shape is a potential approach to evaluating perimeter curvature.

Fourier harmonic analysis of shape has been used to monitor gradual shape changes in sand grains and as a means for discriminating subtle yet distinct populations of various sediments (Ehrlich and Weinberg, 1970). This technique has also been employed successfully in many

Supported in part by grants from the US Department of Agriculture (93-37203-9072 and 98-02163), the National Association of Animal Breeders, and the College of Agricultural and Life Sciences and the Department of Animal Sciences at the University of Wisconsin-Madison.

Correspondence to: Dr John Parrish, Department of Animal Sciences, 1675 Observatory Drive Room 714, Madison, WI 53706 (e-mail: parrish@calshp.cals.wisc.edu).

Received for publication August 15, 2000; accepted for publication January 22, 2001.

different forms to address morphological differences in ostracodes (Kaesler and Waters, 1972), miospores (Christopher and Waters, 1974), murine sperm (Young et al, 1982), epithelial cells, (Kieler et al, 1984), Culicidae wing shapes (Rohlf and Archie, 1984), as well as nuclear and cytoplasmic changes in murine 2-cell embryos (Mystkowska, 1991). Despite successes of Fourier analysis, many investigators continue to rely on measures of length, width, area, and perimeter to distinguish shapes (Gravance et al, 1996; Aziz et al, 1998; Cassidy et al, 1998; Plitt et al, 1999). The reasons for this are probably twofold (Russ, 1995). First, Fourier analysis is computer-intensive and involves comparatively complicated mathematics. Second, shape parameters generated by Fourier analysis are difficult to conceptualize. Nevertheless, inconsistencies among human observers (Dunphy et al, 1989; Neuwinger et al, 1990) and failings of other measures justify the difficulty of using Fourier frequencies and harmonic amplitudes to classify bovine sperm. Objectives of this study were thus to develop methods for fitting Fourier functions to shapes of sperm nuclei; to determine whether Fourier coefficients can be used to distinguish shapes that have previously been described subjectively (eg, tapered, pyriform, macrocephalic, and microcephalic); and to determine whether sperm samples from individual bulls can be distinguished by differences in mean Fourier coefficients.

Materials and Methods

Semen samples

Fresh semen samples from 12 bulls were provided by ABS Global, DeForest, Wisc. The samples were diluted 1:1 in a commercial egg yolk-citrate extender (Pace et al, 1981), transported to the laboratory, and processed within 2 hours of collection. Sperm were removed from seminal fluids and extenders by centrifugation at 15 000 × *g* for 7 seconds, then diluted in 10 mM HEPES-buffered saline (pH 7.4). Sperm concentrations were determined with a hemacytometer and adjusted to 1×10^6 sperm/mL. Sperm from each bull were then placed on 4 long cover slips (24 × 60 mm, number 1), previously coated with 1 mg/ml poly-L-lysine in saline, then air-dried.

Imaging Hardware and Software

Images were visualized using a Nikon Diaphot microscope configured for epifluorescent microscopy. A 75-watt xenon lamp illuminated the samples through a Nikon ND 16 neutral density filter, a 510–560 nm excitation filter, a 580 nm dichroic mirror, and a 590 nm long-pass emission filter. A 100× 1.3 numerical aperture, fluorescent/phase, oil-immersion objective was used in combination with a 1.5× magnifying changer and an intensified Hamamatsu charged coupled device (CCD) camera (Hamamatsu Photonics KK, Sunayama-Cho, Hamamatsu-City, Japan) to capture images. The intensified CCD camera system also included a 2:1 reduction lens to correctly place the image from the intensification screen on the chip within the CCD camera. The final magnification at the level of the camera detection chip was measured at 89× and was based on the observed/actual pixel dimensions. The detail adjustment on the CCD camera controller was set to 12:00. Image analysis was performed on a Gateway 2000 486/25C computer using the Image-1 imaging software (Universal Imaging Corporation, West Chester, Pa). Images acquired by the image analysis system were 8-bit, black-and-white images. The images contained 256 levels of gray at each pixel with black as 0 and white or saturation of a pixel as 255. Various manipulations to image data will be described below to calibrate the system or that were used to identify sperm nuclear perimeters. Detailed descriptions of the mathematics involved in these manipulations, approaches to their use, and image acquisition with CCD cameras can be found in Russ (1995).

Image Collection

Sperm on each coverslip were stained for 5 minutes with 100 μL of 105 μM propidium iodide in 10 mM HEPES-buffered saline. The coverslip was then rinsed and allowed to air-dry. Once stained and dried, a 9-μL drop of glycerol was placed on each coverslip and covered with a smaller, 18 × 18 mm (No 1) coverslip. The 2 coverslips were then sealed together with fingernail polish.

It was observed that the size of sperm nuclei obtained from epifluorescence microscopy and viewed on our image analysis system could be altered by modifying the intensifier sensitivity, the CCD camera gain or offset levels, or the analog to digital converter (ADC) settings within the software. It was further observed that the size of sperm in images obtained from phase-contrast microscopy were not affected by hardware or software settings. The phase-contrast images were therefore used to develop a daily calibration regimen for the epifluorescence portion of the imaging system. At the start of each day, intensifier, camera, and ADC settings were adjusted until images of fluorescently stained sperm nuclei were consistent in size with images of the same sperm captured by phase-contrast microscopy. This was done by acquiring an image of a stained sperm nuclei, closing the shutter of the xenon lamp, and acquiring an image of the same sperm using phase-contrast microscopy. Care was taken to not change the field of view. Using the procedures described in ''Image Processing and Data Collection,'' the fluorescent image was manipulated within the imaging software to threshold and to identify sperm nuclei. This resulted in a binary image in which the background was black and had gray-level values of 0, whereas the sperm were white with a gray-level value of 255. Next, we wished to create an outline of the sperm in the phase-contrast image. To accomplish this a series of image manipulations were required. First, we applied histogram equalization to enhance image contrast. Next, a Sobel operator was applied to the image to identify image regions with high rates of intensity change such as would occur at the edge of a sperm. The resulting image had an outline of each sperm within the image. Finally, a second histogram equalization was applied to better visualize the line created by the Sobel operator. The combination of algorithms resulted in an outline of sperm captured by phase-contrast microscopy. The binary image of the fluorescent sperm nu-

clei was then displayed in red over the modified phase-contrast image displayed in green. The 2 images could be directly compared for consistency in size. When the outline of the phase image and the image of the fluorescent sperm nuclei overlapped, a yellow line was observed around the nucleus, indicating agreement in size and shape of the 2 images. If no yellow line was observed, the image of the fluorescent sperm nuclei was too small. If a yellow line was observed and the image of the fluorescent sperm nuclei extended past the phase image outline, the image of fluorescent sperm nuclei was to large. In both cases, image hardware calibration was considered unsatisfactory and adjustments were made, thereby altering the image of the fluorescent sperm nuclei until the 2 images matched. The calibration routine was performed once at the start of each day. Remaining samples were evaluated without comparison to the phase images.

Image Processing and Data Collection

As light passes through a microscopic sample it is deflected in various directions. In the case of sperm observed by epifluorescent microscopy, the deflection results in the appearance of a halo, a haze, or simply out-of-focus fluorescence light that surrounds each sperm nucleus. To eliminate this artifact from the image, 6 consecutive low-pass filters were executed and the ensuing image was subtracted from the original. Next, binary images were constructed from the enhanced gray-scale images using the automatic threshold algorithm within Image-1. Filters were defined within Image-1 to identify an object as a sperm. These filters were as follows: 15 $\mu m^2 \leq$ area $\leq$ 65 μm^2, 5 $\mu m \leq$ longest chord $\leq$ 20 μm, and 15 $\mu m \leq$ perimeter $\leq$ 40 μm. The Cartesian coordinates (x,y) for the perimeter of each sperm were then acquired and processed using Statistical Analysis System (SAS; version 7-1; SAS Institute, Cary, NC) software to obtain Fourier functions.

Fourier Functions

A series of manipulations within SAS software were made to the perimeter data for each sperm to obtain Fourier functions. The first step was to calculate the centroid as defined by Klecka (1980). The x coordinate of the centroid (Xcent) was defined as the mean of the perimeter x coordinates. The y coordinate of the centroid (Ycent) was defined as the mean of the perimeter y coordinates. The centroid is the center of gravity of an object and the point in which a 2-dimensional object may be balanced on a pin. The perimeter coordinates were then shifted so that the centroid (Xcent,Ycent) was defined as the origin (0,0). The perimeter data were next converted from Cartesian to polar coordinates. Multiple trigonometric regression was then used to partition the perimeter data into a summation of cosines and sines with specific amplitudes and frequencies (Rohlf and Archie, 1984). The Fourier function obtained was of the form:

$$d(\theta) = \sum_{i=0}^{n/2} b_i \cdot \cos(\theta \cdot i) + c_i \cdot \sin(\theta \cdot i), \quad (1)$$

where d is the radial distance from the centroid, θ is the specific angle measured in radians from the positive x-axis, n is the number of perimeter points, i is the trigonometric frequency or harmonic number (the number of times the cosine and sine functions repeat within the interval of 0 to 2π), and b_i and c_i are the computed regression coefficients that identify the amplitude of the cosine and sine frequencies. The Fourier function was then simplified to its condensed form in equation 2:

$$d(\theta) = \sum_{i=0}^{n/2} j_i \cdot \cos(\theta \cdot i - m_i), \quad (2)$$

where

$$j_i = \sqrt{(b_i)^2 + (c_i)^2}, \quad (3)$$

and

$$m_i = \tan^{-1}\left(\frac{c_i}{b_i}\right). \quad (4)$$

The term j_i can be referred to as the amplitude of harmonic i, harmonic amplitude at frequency i, or harmonic amplitude i. These scale the magnitude of their respective cosine frequencies and measure the amount of the frequency present in the original shape of the sperm. The m_is are phase angles that orient or shift the cosine frequencies in relation to one another.

Statistical Analysis

Data were analyzed in SAS using multivariate analysis of variance (MANOVA) based on Wilk's lambda criterion (Bray and Maxwell, 1985), cluster analysis using the average linkage method (Aldenderfer and Blashfield, 1984), and canonical discriminant analysis (Klecka, 1980).

Canonical discriminant analysis is similar to multiple regression with the primary difference being the prediction of the response variable. The analysis constructs a canonical variable, which is a linear combination of the discriminant measures (harmonic amplitudes at frequencies 0–5) that are best at separating the response variable (bulls). Based on the relationship of the discriminant measures with the canonical variable, one can determine which discriminant measures are best at separating the response variable (Klecka, 1980; Jolliffe, 1986).

Results

Attainment of Fourier Functions

Most previous attempts to measure sperm nuclear shape have relied on perimeter data in Cartesian coordinates (x,y), as shown in Figure 1a, c, and e. Although this system is familiar to most researchers, the description of shape based on y as a function of x is difficult to represent mathematically. An alternative approach, shown in Figure 1b, d, and f, is to convert the Cartesian coordinates to polar coordinates (θ,d), where d is the radial distance from the centroid and θ is the angle measured in radians from the positive x axis. This representation is similar to that explained by Kruger et al (1995), except our methods did not require consistent orientation of the sperm (see below). Plots in Figure 1b, d, and f for different sperm show that even small differences in sperm nuclear morphology produce visible changes in $d(\theta)$. It is worthwhile to note that a centroid's location within a sperm nucleus is de-

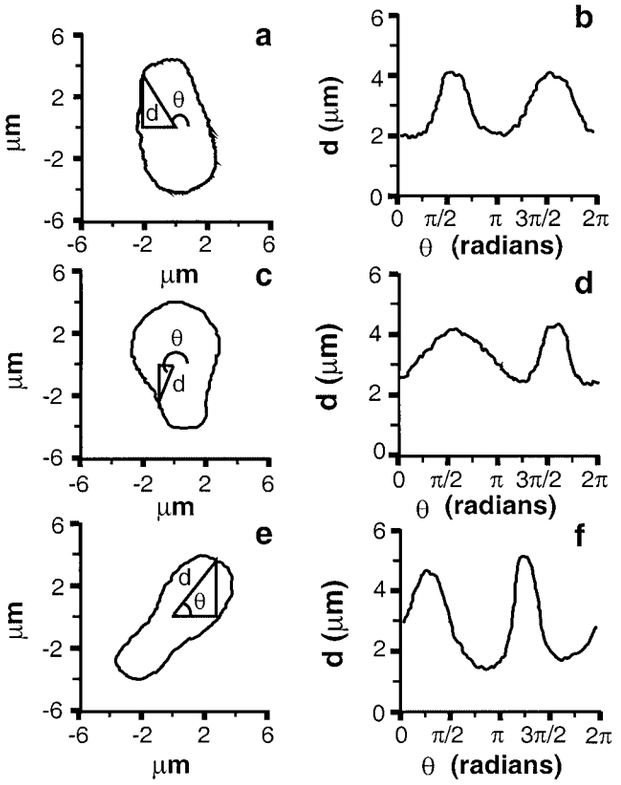

Figure 1. Conversion of Cartesian coordinates to polar coordinates. The graphs in the left column **(a, c,** and **e)** represent the Cartesian coordinates for 3 different sperm. The point of the triangles most near the central point of each sperm is the centroid for that sperm. The right triangle drawn is used to compute the distance, d, and the angle, θ. Plots of θ vs d, shown in panels **(b, d,** and **f)** result in curves that repeat every 2π. Note that each curve is unique and clearly identifies the shape of each sperm's nucleus.

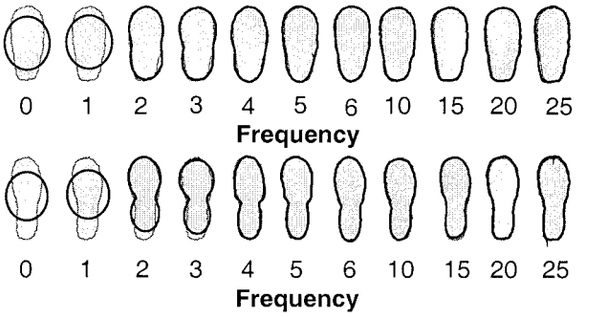

Figure 2. Convergence of Fourier functions to original data. These graphs show the original Cartesian coordinates in gray and the corresponding function, d(θ), in black. The function d(θ) is summed through the frequency indicated by the number below each plot.

pendent on the actual morphology. For example, in a pyriform nucleus, the centroid would be more anterior than it would be in a tapered nucleus. This would reflect the greater mass within the anterior region of a pyriform nucleus. The centroid, however, was used to mathematically define a common central point of reference in each sperm nucleus.

To quantify the changes observed in d(θ) among sperm, a Fourier function was fit (equation 1) to the perimeter data for each sperm and then condensed (equation 2). The resulting function describing sperm nuclear shape was dependent on the Fourier frequencies, harmonic amplitudes, and phase angles. To understand the contribution of Fourier frequencies to sperm nuclear shape, 2 sperm with different nuclear morphology were selected and their calculated functions were summed through various frequencies and superimposed on the original data (Figure 2). These plots demonstrate that the Fourier function starts as a circle, with frequency 0. As additional frequencies are included in the summation, the function diverges from this circle and then converges to the observed data. Figure 2 also illustrates that the types of shape changes associated with each frequency are consistent among sperm. For example, frequencies 0 and 1 are always circles. Frequency 2 always results in elongation. Frequencies 3, 4, and 5 always result in sculpting of the posterior region, while higher order frequencies address finer details. The basis for these consistencies resides in the structure of the condensed Fourier function (equation 2). Note that the frequencies used (i = 0, 1, 2, . . . , n/2) are the same for every sperm.

One of the important features of evaluating shape using the Fourier functions described by equations 1 and 2 is that the magnitude of each Fourier frequency's effect on shape can be quantified by determining the harmonic amplitude (equation 3) at that frequency. Figure 3 demonstrates how the shape of the Fourier function changes as harmonic amplitudes 0–5 are modified. For a randomly selected sperm, the Fourier function was determined through the first 20 frequencies, and this sperm was plotted as the 0% change in Figure 3. The harmonic amplitudes for frequencies 0–5 were determined and, individually, either halved or doubled, while the remaining harmonic amplitudes for the other frequencies were left unchanged. Thus, the effect on nuclear shape of the harmonic amplitude at a single frequency could be visualized. Manipulating harmonic amplitude 0 changed the overall size of the nucleus. A smaller harmonic amplitude 0 reflects a sperm with smaller overall size. A larger harmonic amplitude 0 reflects a sperm with larger over all size. Harmonic amplitude 1 changed the rounding of the anterior portion of the nucleus. This is only a subtle effect, which is visibly better with greater magnification (not shown). This indicates that frequency 1 has very little effect on the overall shape of the sperm nucleus, but as harmonic amplitude 1 increases, there is increased rounding in the anterior portion of the nucleus. Elongation is measured by harmonic amplitude 2. Harmonic amplitudes

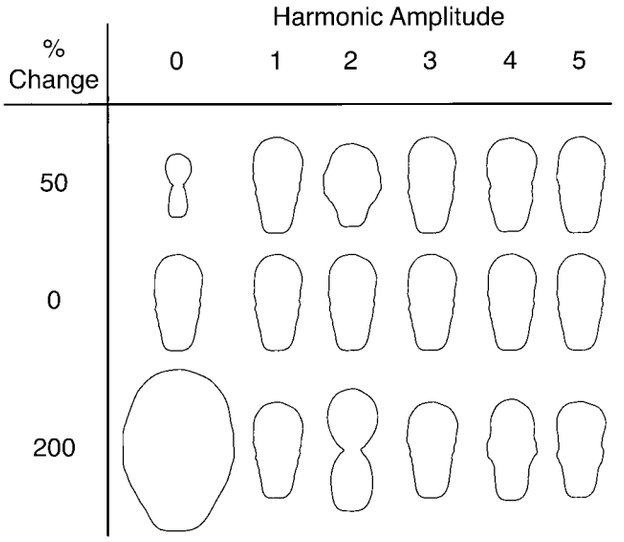

Figure 3. Changes in the Fourier function by varying harmonic amplitude values at frequencies 0–5. The center row (0% change) shows the Fourier function of a randomly selected sperm summed through 20 frequencies. The top and bottom rows illustrate how the Fourier function in the center row changes when the harmonic amplitude for the specific frequency at the top of each column is changed by 50% or 200%, respectively. When the value of the specific harmonic amplitudes was changed, the harmonic amplitude values at the other frequencies remained unchanged.

3–5 measure tapering of progressively more-caudal portions of the posterior half of the nucleus. It is important to remember that the approach used in Figure 3 was undertaken to visualize the effect of individual harmonic amplitudes on the overall nuclear shape. In reality, the magnitude of the harmonic amplitudes at the specific frequencies change in concert with one another to describe different nuclear shapes.

In theory, Fourier harmonic amplitudes should be independent of object orientation (Younker and Ehrlich, 1977). To determine if this was true for harmonic amplitudes obtained from sperm nuclei, perimeter points were obtained for a single sperm, rotated about its centroid, then condensed Fourier functions were calculated. The orientation of the sperm, harmonic amplitudes, and phase angles obtained are shown in Figure 4 and Table 1, respectively. The harmonic amplitude values (j_i in Table 1) were independent of sperm orientation. In contrast, the values obtained for phase angles (m_i) changed as the sperm was rotated.

As the number of frequencies used in the condensed Fourier function increases, the residuals decrease until at n/2, where n is the number of data points defining the object's perimeter, the function exactly recreates the original data (Nyquist Theorem, cited by Bloomfield, 1976). In this study, n typically ranged from 200 to 300. Because relatively ''coarse'' shape change such as roundness,

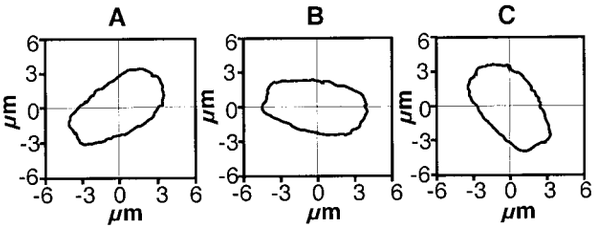

Figure 4. Independence of harmonic amplitudes and sperm orientation. The Cartesian coordinates obtained for the image in graph **(A)** were rotated clockwise about the origin $\pi/4$ (graph **B**) and $3\pi/2$ (graph **C**) radians. The harmonic amplitudes and phase angles were calculated through the 20th frequency and the values obtained appear in Table 1.

elongation, and/or taperedness occur with the lower-order frequencies, and higher-order frequencies reflect changes in ''fine'' surface details (Figure 2), at some point higher-order frequencies should reflect edge variations due to the image acquisition process. Thus, to determine a point at which to truncate the Fourier series the resolution capabilities of the digitizing equipment were next addressed. To accomplish this, 5 different sperm were imaged and redigitized 5 consecutive times. The coefficients of variation (CV) for each sperm's harmonic amplitudes, 0 to 31, were computed and displayed in Figure 5. The variation in the CVs obtained for harmonic amplitudes 0–5 were relatively low when compared with those for 6–31. This infers inconsistencies from one digitization to the next in the values obtained for harmonic amplitudes 6–31. To describe bovine sperm nuclei, Fourier series were truncated to 6 harmonics (ie, frequencies 0 to 5). Visual inspection of Figure 2 confirms that sperm nuclear shape is essentially described by $d(\theta)$ when frequencies 0–5 were used. This truncation resulted in a multivariate observation for each sperm containing 6 variables that may be used to quantify and assess sperm nuclear shape independent of orientation.

A property of Fourier functions are that if the data (pe-

Table 1. *Harmonic amplitude (j_i) and phase angles (m_i) calculated for various frequencies (i) and sperm orientations shown in Figure 3**

	Corresponding Panel in Figure 4					
	A		B		C	
i	j_i	m_i	j_i	m_i	j_i	m_i
0	3.184	0.000	3.184	0.000	3.184	0.000
1	0.041	1.887	0.041	1.101	0.041	3.458
2	0.995	1.197	0.995	5.910	0.995	4.338
3	0.128	4.477	0.128	2.121	0.128	2.906
4	0.167	2.523	0.167	5.664	0.167	2.523
5	0.068	5.921	0.068	1.994	0.068	1.209
10	0.023	2.015	0.023	0.444	0.023	5.156
15	0.019	2.649	0.019	3.435	0.019	1.079
20	0.008	1.923	0.008	5.065	0.008	1.923

* Harmonic amplitudes measured in μm, phase angles measured in radians.

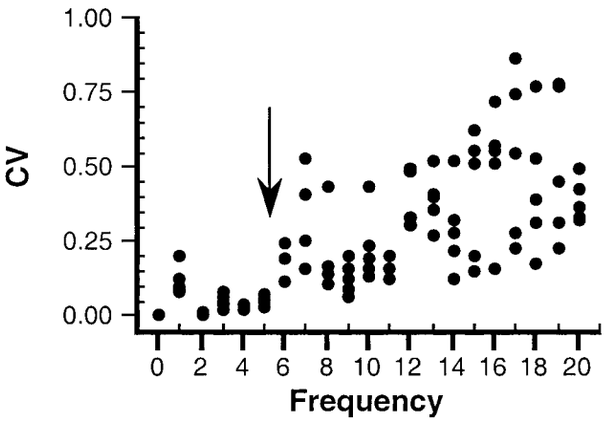

Figure 5. Determination of Fourier series truncation. Because an excess of 100 frequencies could have been used in the summation of d(θ), it was desirable to limit the number of frequencies needed. This graph shows the coefficients of variation (CV = $\sigma/\bar{x}$) obtained when 5 different sperm were imaged 5 consecutive times for frequencies 0 to 31. The arrow indicates the truncation point.

rimeter points) are evenly spaced (eg, every 3 degrees or 0.05 radians), the cosine frequencies are orthogonal (Russ, 1991). Each of the harmonic amplitudes will measure an independent aspect of the original shape and will not depend upon its predecessors. In this experiment we chose to use each perimeter pixel as a data point. Due to the curvature of the sperm, the data obtained are at unevenly spaced angles. There is a small but significant correlation among the cosine frequencies ($r < .04$; $P < .05$). Regardless, each of the harmonic amplitudes measures a unique aspect of shape and can be compared among sperm.

Assessment of Fourier Harmonic Amplitudes as Sperm Nuclear Shape Descriptors

To determine if harmonic amplitudes from Fourier functions could be used to detect differences in sperm nuclear shape, 1816 sperm from 12 bulls were imaged. The perimeter points for each sperm were determined, and harmonic amplitudes for frequencies 0–5 were calculated. The mean ± SD for harmonic amplitudes 0–5 for each bull are shown in Table 2. MANOVA found that harmonic amplitudes differed among bulls ($P < .05$).

Cluster analysis was next performed on the same sperm harmonic amplitudes to identify 20 different clusters. Randomly selected sperm from each cluster along with the number of sperm in that cluster are shown in Figure 6. By definition, cluster analysis separates entities into clusters that have no overlap along the variables used to create them. Thus, if MANOVA is performed, the clusters are always shown to be statistically different from one another (Aldenderfer and Blashfield, 1984). This is supported by visual inspection of Figure 6. The 3-dimensional graph shows that sperm within a cluster have similar harmonic amplitude combinations and that sperm from different clusters occupy unique volumes. When sperm were randomly selected, those within a cluster had similar nuclear shapes, whereas those from different clusters possessed distinctive shape characteristics. The percentages of the 1816 sperm in each cluster were as follows: cluster 1, 94.2%; cluster 2, 0.2%; cluster 3, 0.6%; cluster 4, 1.2%; cluster 5, 0.9%; cluster 6, 0.6%; cluster 7, 0.8%; cluster 8, 0.2%; cluster 9, 0.2%; clusters 10–20, 1.0%.

The majority of sperm evaluated were identified as belonging to cluster 1 (94%). On the basis of the shape of the randomly selected sperm from this cluster, these sperm would have been classified as normal using the procedures of conventional semen evaluation (Figure 6). To determine how cluster analysis would subdivide the sperm in cluster 1, a second cluster analysis was used to separate the 1710 sperm originally assigned to cluster 1 into 10 unique subclusters (Figure 7). The percentages of sperm placed into each new cluster were as follows: cluster 1, 46.4%; cluster 2, 6.7%; cluster 3, 11.9%; cluster 4, 19.1%; cluster 5, 5.3%; cluster 6, 7.5%; cluster 7, 2.1%; cluster 8, 0.4%; cluster 9, 0.5%; cluster 10, 0.05%. As shown by the scatter plot, the subclusters occupied unique volumes within the space used to assess sperm nuclear shape. However, because the distances from one subcluster to the next were less than those observed in Figure 6, it was much more difficult to perceive nuclear shape differences among the randomly selected sperm from the subclusters. Nevertheless, the harmonic amplitude combinations outlined by the cluster analysis resulted in statistically unique groups.

Discussion

An objective and repeatable method to evaluate the morphology of sperm nuclei was developed using Fourier harmonic analysis. To ensure accuracy and repeatability, substantial time and effort were devoted to the development of methodology. Epifluorescent microscopy was used to obtain images of propidium iodide-stained sperm to circumvent the need to eliminate the sperm tails either before or during image analysis, or both. To ensure that sperm were lying flat during image collection, sperm were attached to coverslips coated with poly-L-lysine and dried. Because the bovine sperm head is essentially shaped like a paddle (8–10 μm long by 4 μm across and 1 μm thick; Salisbury and VanDemark, 1961), binding to poly-L-lysine followed by drying ensured that the sperm attached to the coverslip with the largest amount of surface area possible (ie, flat). Epifluorescent microscopy presented unique problems in repeatable quantification of

Table 2. *Differences among bulls in harmonic amplitudes (mean ± SD) at Fourier frequencies 0–5**

Bull	Sperm Evaluated	Harmonic Amplitude Frequency 0	1	2	3	4	5
1	174	3.20 ± 0.09	0.15 ± 0.04	1.12 ± 0.09	0.17 ± 0.04	0.22 ± 0.05	0.10 ± 0.03
2	170	3.17 ± 0.11	0.15 ± 0.07	1.20 ± 0.10	0.14 ± 0.06	0.26 ± 0.07	0.14 ± 0.05
3	251	3.14 ± 0.12	0.13 ± 0.04	1.13 ± 0.10	0.16 ± 0.05	0.21 ± 0.06	0.09 ± 0.03
4	245	3.10 ± 0.09	0.13 ± 0.04	1.21 ± 0.09	0.13 ± 0.04	0.27 ± 0.06	0.10 ± 0.03
5	228	3.15 ± 0.09	0.13 ± 0.03	1.13 ± 0.07	0.15 ± 0.03	0.18 ± 0.05	0.10 ± 0.03
6	181	3.14 ± 0.10	0.13 ± 0.05	1.19 ± 0.08	0.12 ± 0.04	0.28 ± 0.07	0.12 ± 0.04
7	95	3.05 ± 0.10	0.12 ± 0.04	1.04 ± 0.10	0.16 ± 0.05	0.17 ± 0.05	0.09 ± 0.03
8	57	3.02 ± 0.14	0.15 ± 0.07	1.30 ± 0.12	0.13 ± 0.05	0.34 ± 0.11	0.13 ± 0.06
9	72	2.93 ± 0.11	0.10 ± 0.03	1.14 ± 0.07	0.10 ± 0.04	0.26 ± 0.05	0.07 ± 0.03
10	81	3.19 ± 0.09	0.19 ± 0.05	1.15 ± 0.10	0.21 ± 0.06	0.26 ± 0.07	0.13 ± 0.04
11	134	3.24 ± 0.12	0.14 ± 0.03	1.22 ± 0.09	0.14 ± 0.04	0.26 ± 0.05	0.11 ± 0.03
12	128	3.22 ± 0.09	0.16 ± 0.04	1.16 ± 0.08	0.17 ± 0.04	0.25 ± 0.06	0.11 ± 0.04

* Differences among these 12 randomly selected bulls were found in sperm nuclear shape as judged by mean harmonic amplitude at frequencies 0–5 using MANOVA; $p < .05$). The MANOVA approach was used because the harmonic amplitudes at each frequency were separate response variables and correlations would likely be present.

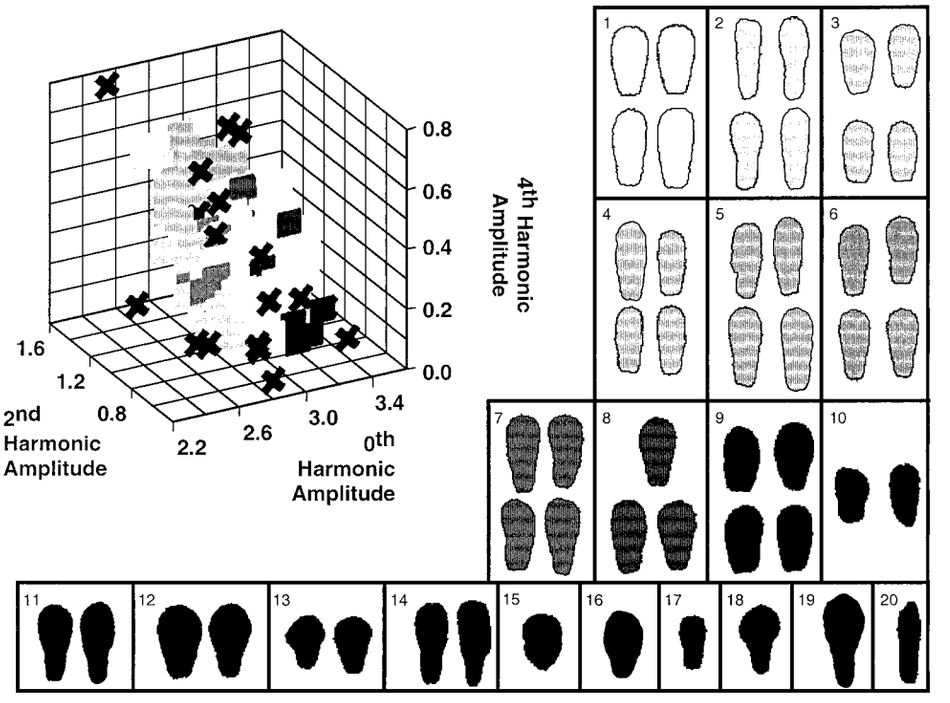

Figure 6. Cluster analysis of harmonic amplitudes. The harmonic amplitudes at frequencies 0–5 for the 1816 sperm nuclei evaluated in Table 2 were evaluated here by cluster analysis without regard to bull. Although 6-dimensional space can be dealt with mathematically, it cannot be represented graphically. Thus, in order to view the data, the best approach available was to construct a scatter plot in 3 dimensions. To select the most suitable 3 dimensions, a canonical discriminant analysis was used to determine which harmonic amplitudes had the greatest discriminating power between the bulls used in this study. Using a variable selection technique similar to one proposed for principal component analysis (Jolliffe, 1986), those discriminant parameters with the lowest canonical correlation to the last discriminant function were chosen. The scatter plot indicates the location of each sperm in only 3 dimensions, while its group assignment based on harmonic amplitudes 0–5 is represented by its gray level. Those sperm contained within a box are from the cluster indicated by the number, and the shade of the sperm coincides with the shade in the scatter plot. Within the scatter plot, cluster 9 is represented by black squares, whereas clusters 10–20 are represented by black x's. The number of sperm placed into each cluster is as follows: cluster 1, n = 1710; cluster 2, n = 4; cluster 3, n = 11; cluster 4, n = 22; cluster 5, n = 16; cluster 6, n = 11; cluster 7, n = 16; cluster 8, n = 3; cluster 9, n = 4; clusters 10–20, n = 19.

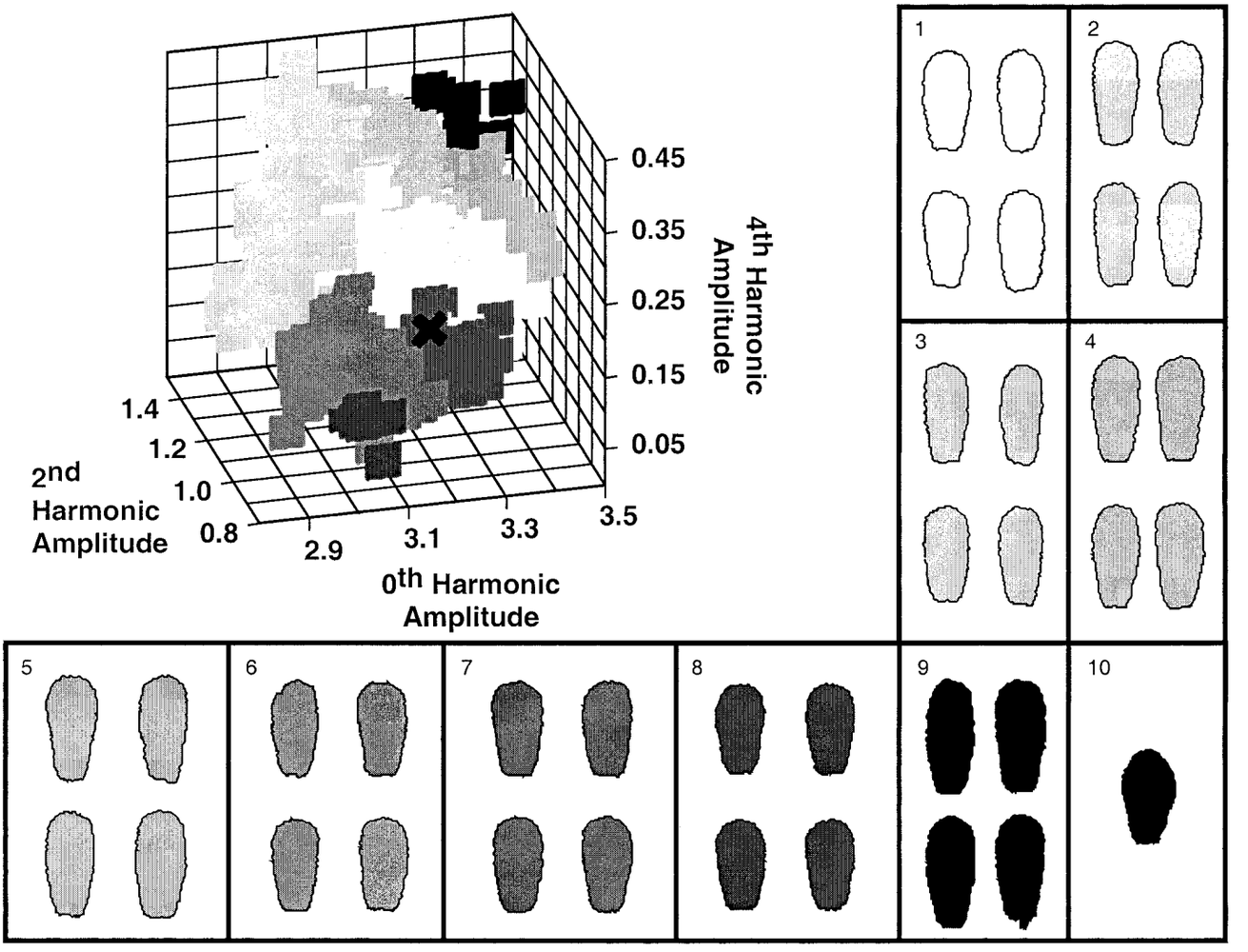

Figure 7. Cluster analysis of harmonic amplitudes from sperm most likely to have been classified as normal using conventional semen analysis procedures. Those 1710 sperm previously grouped together as cluster 1 in Figure 6 were subdivided using a second cluster analysis. The scatter plot indicates the location of each sperm in only 3 dimensions, whereas its group assignment based on all harmonic amplitudes, 0–5, is represented by its gray level. Those sperm contained within a box are from the cluster indicated by the number, and the shade of the sperm coincides with the shade in the scatter plot. Within the scatter plot, cluster 9 is represented by black squares, whereas cluster 10 is represented by a single black x. The number of sperm placed into each cluster is as follows: cluster 1, n = 794; cluster 2, n = 115; cluster 3, n = 203; cluster 4, n = 326; cluster 5, n = 91; cluster 6, n = 129; cluster 7, n = 36; cluster 8, n = 7; cluster 9, n = 8; cluster 10, n = 1.

images as the edge of fluorescent objects was dependent on sensitivity settings of the detection camera. We developed a novel method to calibrate the sensitivity of our digital camera each day by using the intensifier sensitivity along with the camera gain, and offset controls to ensure that epifluorescent images of sperm nuclei were the same size as the respective phase-contrast images of the corresponding sperm heads. Although using this method may result in enlarging the sperm nucleus to the size of the plasma membrane, the effect was minor at best and likely below the resolution of the imaging system. There was likely no effect of the acrosome on the calibration as all sperm acrosome-reacted during the drying phase of slide preparation. It must be emphasized that the unique aspects of imaging fluorescence required calibrating the sensitivity of the imaging system on a daily basis if quantitative data were to be obtained.

The form of the Fourier harmonic analysis represented by equations 1 and 2 assesses the curvature of an object's perimeter in relation to its centroid. Other forms do exist, and may be better suited for more irregular or indented perimeters in which any given radius may cross the perimeter at multiple points (Rohlf and Archie, 1984; Diaz et al, 1989). However, because this was not a concern for

bovine sperm nuclei, the simpler method based on polar coordinates was used. The Fourier functions as we describe them may also have frequencies up to ½ the number of perimeter points. In our case, the Fourier functions were able to describe shape detail in excess of the imaging resolution. However, only harmonic amplitudes for frequencies 0–5 were needed to describe the shape of bovine sperm.

While the mathematical aspects of sperm nuclear shape addressed by each harmonic amplitude can be described in terms of the function $d(\theta)$, it can be difficult to explain these components using common terms of sperm nuclear shape. However, general conclusions about the contribution of each frequency and its corresponding harmonic amplitude to the overall shape of sperm heads was possible. Based on these conclusions, predictions about changes in harmonic amplitudes with different types of sperm abnormalities can be made. For example, because harmonic amplitude 0 measures overall sperm size, it should be less for microcephalic sperm and greater for macrocephalic sperm when compared with normal sperm. Harmonic amplitude 1 measures the roundness of the anterior head and should be larger for pyriform-shaped sperm. Harmonic amplitude 2 measures sperm length and should also be different for microcephalic and macrocephalic sperm. Harmonic amplitudes 3, 4, and 5 measure the shaping of the posterior head and should differ for pyriform and tapered sperm. In fact, when sperm were grouped based solely on their harmonic amplitudes 0–5, some of the clusters appeared to have identified sperm abnormalities that have been previously described (Figure 6; Barth and Oko, 1989). Sperm in clusters 2, 3, 4, and 8 were tapered, microcephalic, macrocephalic, and pyriform, respectively. Thus, the predictions made about the contributions of individual harmonic amplitudes were confirmed by the location of abnormally shaped sperm in the 3-dimensional scatter plot of Figure 6.

One powerful aspect of Fourier harmonic analysis of shape is its ability to recreate the original shape. This includes asymmetrical shapes such as those seen in bovine sperm. In this sense, the asymmetry exists from the anterior to posterior regions of the sperm, with the anterior region generally being larger. If asymmetry exists from left to right, the Fourier function will also reflect this as well, as the curve explained by the Fourier function, $d(\theta)$, exists from θ equal to $0–2\pi$. This would account for the entire sperm nucleus.

We confirmed that Fourier harmonic amplitudes were independent of sperm orientation, as predicted from theory (Younker and Ehrlich, 1977). This is an important and unique aspect of our approach to shape measurement that would simplify potential automation. A question that still remains is whether the phase angles of the condensed Fourier functions contain any further information on shape (Flook, 1982). Any comparison of phase angles would require the consistent orientation of sperm prior to evaluation, and in the current studies this was not done. A plot of the mean sperm shape may be advantageous in order to visualize mean sperm head shape from different bulls. Again, because this would require obtaining average phase angles and sperm orientation, we did not attempt this in the present study.

Differences among bulls in the harmonic amplitude centroids were encouraging because they may enable us to relate sperm morphology to bull fertility. We further demonstrated that cluster analysis of harmonic amplitudes could objectively identify sperm shapes that have previously been identified as abnormalities in bovine sperm. Therefore, it would be feasible to use a discriminant analysis to determine a linear combination of harmonic amplitudes to best separate these predefined categories of sperm nuclear shape. The resulting discriminant function could then be used to objectively classify sperm into normal or various categories of abnormal. In essence, this strategy would be quite similar to those in which semen evaluation systems are ''trained'' to place sperm into various morphological categories based on various measures that include length, width, and area (Kruger et al, 1995; Steigerwald and Krause, 1998; Coetzee et al, 1999). Although an increased precision of classification would be expected, subjectivity would still be present. In using this type of approach, subjectivity would be introduced when deciding how to classify sperm for the training data set that would be used to construct the discriminate function. We propose a novel and more robust use of Fourier harmonic amplitudes.

In general, previous methods to evaluate sperm head morphology have produced categorical data, as sperm are typically placed into groups representing various categories of normal and abnormal (Wang et al, 1991; Ferrari et al, 1998; Sukcharoen et al, 1998). Fourier harmonic analysis, as proposed here, is different in several respects. First, it produces continuous data that can be used to better explain sperm nuclear shape distributions. For example, in this study, sperm nuclear shape within a bull was explained in terms of means and standard deviations for specific harmonic amplitudes, as seen in Table 2. However, other characteristics of the distribution such as the median, mode, skewness, kurtosis, and or the covariances among the harmonic amplitudes may prove to be more useful for semen evaluation. Second, the approach used here makes no distinction as to the normality status of a particular sperm. This last point is particularly important. A common problem with current methods used to evaluate sperm morphology is that they are subjective and they depend on the opinions of individual people classifying the sperm (Dunphy et al, 1989; Neuwinger et al, 1990). In the current study, great care was taken to intro-

duce as few biases as possible, because little is actually known about the relationship between sperm head shape and bull fertility. In fact, Barth et al (1992) showed that a bull producing high numbers of ''abnormally'' tapered sperm was more fertile than a control bull that produced high numbers of ''normally'' shaped sperm. Thus, it may be that some types of sperm previously considered abnormal may have positive effects on fertility. This is exactly why we let the harmonic amplitudes alone identify groups and subgroups of sperm head shapes (Figures 6 and 7). In addition, these measures were able to establish differences among bulls in mean sperm head shape ($P < .05$; Table 2). Such objectivity may eventually allow us to identify novel sperm head shapes, distribution characteristics, or a combination of these, that affect male fertility.

In summary, it has been shown that computer-aided image analysis can be used to obtain Fourier functions and thus, harmonic amplitudes from sperm stained with propidium iodide. The harmonic amplitudes can be used to assess sperm nuclear shapes previously reported, as well as gradations in between. Furthermore, these measures were shown to be independent of sperm orientation, quite sensitive to slight alterations in sperm nuclear shape, and were able to distinguish differences in mean sperm nuclear shape between bulls.

Acknowledgments

The authors thank ABS Global for their generous donation of the semen used in this study. Furthermore, we thank Dr Erik V. Nordheim, Dr Chongqing Yan, and Mr Peter Crump, as well as the rest of the CALS Biometry Department for their help and discussion in design and analysis of the work presented.

References

Aldenderfer MS, Blashfield RK. *Cluster Analysis.* Sage University Paper Series on Quantitative Applications in the Social Sciences, Series 07-044. Beverly Hills, Calif: Sage Publications; 1984.

Atteneave F. Some information aspects of visual perception. *Psychol Rev.* 1954;61:183–193.

Atteneave F, Arnoult MD. The quantitative study of shape and pattern perception. In: Uhr L, ed. *Pattern Recognition.* New York, NY: Wiley and Sons; 1966: 123–141.

Auger J, Dadoune JP. The nuclear status of human sperm cells by TEM image cytometry: changes in nuclear shape and chromatin texture during spermiogenesis and epididymal transit. *Biol Reprod.* 1993;49: 166–175.

Aziz N, Fear S, Taylor C, Kingsland C, Lewis-Jones D. Human sperm head morphometric distribution and its influence on human fertility. *Fertil Steril.* 1998;70:883–891.

Barth AD, Bowman PA, Gabriel AB, Mapletoft RJ. Effect of narrow sperm head shape on fertility in cattle. *Can Vet J.* 1992;33:31–39.

Barth AD, Oko RJ. Defects of the sperm head. In: Barth AD, Oko RJ, eds. *Abnormal Morphology of Bovine Spermatozoa.* Ames: Iowa State University Press; 1989: 130–192.

Berkovitz A, Eltes F, Soffer Y, Zabludovsky N, Beyth Y, Farhi J, Levran D, Bartoov B. ART success and in vivo sperm cell selection depend on the ultramorphological status of spermatozoa. *Andrologia.* 1999; 31:1–8.

Bloomfield P. The search for periodicity. In: Bloomfield P, ed. *Fourier Analysis of Time Series: An Introduction.* New York, NY: John Wiley and Sons; 1976: 9–42.

Bray JH, Maxwell SE. *Multivariate Analysis of Variance.* Sage University Paper Series on Quantitative Applications in the Social Sciences, Series 07-054. Beverly Hills, Calif: Sage Publications; 1985.

Cassidy KM, Harris EF, Tolley EA, Keim RG. Genetic influence on dental arch form in orthodontic patients. *Angle Orthodontist.* 1998;68:445–454.

Christopher RA, Waters JA. Fourier series as a quantitative descriptor of miospore shape. *J Paleontol.* 1974;48:697–709.

Coetzee K, Kruger T, Lombard C, Shaughnessy D, Oehninger S, Ozgur K, Pomeroy K, Muller C. Assessment of interlaboratory and intralaboratory sperm morphology reading with the use of a Hamilton Thorne Research integrated visual optical system semen analyzer. *Fertil Steril.* 1999;71:80–84.

Diaz G, Zuccarelli A, Pelligra I, Ghiani A. Elliptic Fourier analysis of cell and nuclear shapes. *Comp Biomed Res.* 1989;22:405–414.

Dunphy BC, Kay R, Barratt CLR, Cooke ID. Quality control during the conventional analysis of semen, an essential exercise. *J Androl.* 1989; 10:378–385.

Ehrlich R, Weinberg B. An exact method for characterization of grain shape. *J Sedim Petrol.* 1970;40:205–221.

Ferrari M, Spirito S, Giuliano S, Fernandez H. Chromatin cytophotometric analysis of abnormal bovine spermatozoa. *Andrologia.* 1998; 30:85–89.

Flook AG. Fourier analysis of particle shape. In: Stanly-Wood NG, Allen T, eds. *Particle Size Analysis.* Chinchester, NY: Wiley Heyden Ltd; 1982: 255–262.

Gravance C, Liu I, Davis R, Hughes J, Casey P. Quantification of normal head morphometry of stallion spermatozoa. *J Reprod Fertil.* 1996; 108:41–46.

Johnson K, Dewey C, Bobo J, Kelling C, Junstra D. Prevalence of morphologic defects in spermatozoa from beef bulls. *J Am Vet Med Assoc.* 1998;213:1468–1471.

Jolliffe IT. Choosing a subset of principal components or variables. In: *Principal Component Analysis.* Springer Series in Statistics. New York, NY: Springer-Verlag; 1986: 92–114.

Katz DF, Davis RO. Automatic analysis of human sperm motion. *J Androl.* 1987;8:170–181.

Kaesler RL, Waters JA. Fourier analysis of the ostracode margine. *Geol Soc Am Bull.* 1972;83:1169–1178.

Kieler J, Ostrowski K, Strojny P, Rozycka M, Dziedzic-Goclawsk A, Bulski W. Fourier analysis of the shape of normal and transformed epithelial cells derived from human transitional epithelium. *Histochemistry.* 1984;81:119–128.

Klecka WR. *Discriminant Analysis.* Sage University Paper Series on Quantitative Application in the Social Sciences, Series 07-019. Beverly Hills, Calif: Sage Publications; 1980.

Kruger T, Toit T, Franken D, Menkveld R, Lombard C. Sperm morphology: assessing agreement between the manual method (strict criteria) and the sperm morphology analyzer IVOS. *Fertil Steril.* 1995;63: 134–141.

Lim C, Lewis S, Kennedy M, Donnelly E, Thompson W. Human sperm morphology and in vitro fertilization: sperm tail defects are prognostic for fertilization failure. *Andrologia.* 1998;30:43–47.

Makler A. A new multiple exposure photography method for objective human spermatozoal motility determination. *Fertil Steril.* 1978;30: 192–199.

Mystkowska ET, Komar A, Strojny P, Rozycka M, Sawicki W. Fourier

analysis of the nuclear and cytoplasmic shapes of living two-cell murine embryos. *Anal Quant Cytol Histol.* 1991;13:209–214.

Neuwinger J, Behre H, Nieschlag E. External quality control in the andrology laboratory: an experimental multicenter trial. *Fertil Steril.* 1990;54:308–314.

Pace MM, Sullivan JJ, Eliott FI, Graham EF, Coulter GH. Effects of thawing temperature, number of spermatozoa and spermatozoal quality on fertility of bovine spermatozoa packaged in 0.5 ml French straws. *J Anim Sci.* 1981;53:693–701.

Park K, Yi W, Paick J. Segmentation of sperms using the strategic Hough transform. *Ann Biomed Eng.* 1997;25:294–302.

Plitt A, Imarom S, Joachim A, Daugschies A. Interactive classification of porcine *Eimeria* spp. by computer-assisted image analysis. *Vet Parasitol.* 1999;86:105–112.

Rohlf FJ, Archie JW. A comparison of Fourier methods for the description of wing shape in mosquitoes (*Diptera*: Culicidae). *Syst Zool.* 1984; 33:302–317.

Russ JC. Harmonic analysis. In: *Computer-Assisted Microscopy: The Measurement and Analysis of Images.* New York, NY: Plenum Press; 1991: 206–210.

Russ JC. *The Image Processing Handbook.* 2nd ed. Boca Raton, Fla: CRC Press; 1995.

Salisbury GW, Beck GH, Elliott I, Willet EL. Rapid methods for estimating the number of spermatozoa in bull semen. *J Dairy Sci.* 1943; 26:69–78.

Salisbury GW, VanDemark NL. Morphology and motility of spermatozoa. In: *Physiology of Reproduction and Artificial Insemination of Cattle.* San Francisco, Calif: WH Freeman; 1961: 232–258.

Sailer BL, Jost LK, Evenson DP. Bull sperm head morphometry related to abnormal chromatin structure and fertility. *Cytometry.* 1996;24: 167–173.

Steigerwald P, Krause W. Estimation of sperm morphology using a new CASA system. *Andrologia.* 1998;30:23–27.

Sukcharoen N, Sithipravej T, Promviengchai S, Chinpilas V, Boonkasemsanti W. Sperm morphology evaluated by computer (IVOS) cannot predict the fertilization rate in vitro after intracytoplasmic sperm injection. *Fertil Steril.* 1998;69:564–568.

Wang C, Leung A, Tsoi WL, Leung J, Ng V, Lee KF, Chan SY. Computer-assisted assessment of human sperm morphology: comparison with visual assessment. *Fertil Steril.* 1991;55:983–988.

Willet EL, Buckner PJ. The determination of numbers of spermatozoa in bull semen by measurement of light transmission. *J Anim Sci.* 1951; 10:219–225.

Young IT, Gledhill BL, Lake S, Wyrobek AJ. Quantitative analysis of radiation-induced changes in sperm morphology. *Anal Quant Cytol.* 1982;4:207–216.

Young IT, Walker JE, Bowie JE. An analysis technique for biological shape. I. *Inform Control.* 1974;25:357–370.

Younker JL, Ehrlich R. Fourier biometrics: harmonic amplitudes as multivariate shape descriptors. *Syst Zool.* 1977;26:336–342.